Few-particle energies versus geometry and composition of $In_xGa_{1-x}As/GaAs$ self-organized quantum dots

Andrei Schliwa,* Momme Winkelnkemper, and Dieter Bimberg
Institut für Festkörperphysik, Technische Universität Berlin, Hardenbergstr. 36, 10623 Berlin, Germany
(Received 5 February 2008; revised manuscript received 16 December 2008; published 27 February 2009)

Energies of exciton, biexciton, and charged excitons for a large variety of realistic quantum dots are calculated using the configuration-interaction model in conjunction with eight-band $\mathbf{k}\cdot\mathbf{p}$ theory. The interrelation between quantum dot (QD) geometry and composition, the resulting shape and position of electron and hole wave functions, the direct Coulomb energies, and the changes introduced by correlation effects are analyzed in detail. The QD size, the base shape—being either circular, square, or rhombohedral—and the vertical and lateral aspect ratio are varied. Different average compositions and composition profiles, such as the "trumpet shape," or an isotropic In gradient resulting from postgrowth annealing processes are studied. The resulting spectroscopic signatures turn out to be very sensitive to all these structural and chemical parameters. We analyze their interrelation to address the band-structure inversion problem, gaining information on the QD morphology from its spectroscopic signature. The results are compared to available experimental data.

DOI: 10.1103/PhysRevB.79.075443 PACS number(s): 73.21.La, 71.35.Cc, 71.70.−d, 77.65.Ly

I. INTRODUCTION

Single quantum dot (QD) spectroscopy reveals the energetics of excitonic complexes, such as the exciton X^0,[1] the biexciton XX^0,[2–4] or charged excitons, i.e., positive and negative trions $X^{\pm}$.[5–8] In their respective ground states only the lowest electron and hole levels are occupied. Without Coulomb interaction, the recombination energies of these particles would be identical. In experiment, however, these energies are not degenerate but split by several meV. Moreover, their energetic ordering differs for different QD sizes and shapes. Hence, a connection between the energy of the different excitonic complexes and the morphology of the QDs has to be established. The Coulomb interaction within the few-particle complexes, including exchange and correlation effects, is here of large importance. To address this matter we calculate the recombination energies of exciton, biexciton, and both trions for a large number of QDs, varying their size, shape (square/circular/rhomboid base and different vertical/lateral aspect ratios), and composition (homogeneous/peaked and isotropic interdiffusion).

The QD structure affects the confinement potential not only by its own geometry and composition profile but also via the inhomogeneous strain and piezoelectricity. As a result, electron and hole ground-state orbitals can differ in their respective size, shape, and center-of-mass position, leading to different magnitudes of the direct Coulomb interaction for different pair interactions (electron-electron, electron-hole, and hole-hole). This mechanism alone gives rise to different recombination energies for particles $X^0, XX^0, X^{\pm}$. However, only four ordering schemes for the four resonances can be found by accounting direct Coulomb interaction terms only. These schemes, e.g., exclude the existence of a binding biexciton which appears on the low-energy side of the exciton resonance. This case, however, is often observed in experiment and demands the inclusion of further Coulomb contribution, such as self-consistency and, in particular, correlation effects, being achieved by employing the configuration-interaction (CI) model. In this model the many-particle Hamiltonian is expanded into a set of Slater determinants formed by single-particle wave functions.[9] In a strong-confinement system, where the Coulomb energies are small compared to the quantization energies, the single-particle states from the unperturbed system (absence of Coulomb interaction) pose an excellent choice for building up the many-particle basis set. For their calculation we use the eight-band $\mathbf{k}\cdot\mathbf{p}$ model, which enables us to calculate the electronic structure of arbitrarily shaped QDs, accounting for strain, as well as for piezoelectricity (first and second orders[10,11]) and band-mixing effects.[12] The model provides, at reasonable computational cost, a fast and transparent relation between the electronic structure of QDs and bulk properties of the constituent materials.

Once the Hamiltonian is expanded into the basis of Slater determinants formed by eight-band $\mathbf{k}\cdot\mathbf{p}$ orbitals, the resulting matrix is diagonalized and the few-particle energies are obtained. A true self-consistency step is not a necessary part of this model; its effect, however, is largely incorporated. By employing the CI method, we account for direct Coulomb effects, exchange, and large parts for self-consistency effects and correlation.

Despite the tremendous advances in structural characterization techniques, the real shape and composition of capped QDs, which present the decisive input parameters for all modeling,[12–14] are often only poorly known. Even the most sophisticated techniques provide either cross-section images of capped[15,16] or surface images of uncapped[17,18] QDs. The paper will show that specific spectroscopic properties, namely, the binding energies of $X^{\pm}$ and XX relative to the exciton ground state are very sensitive to the geometry and composition of QDs. Therefore, these quantities are fingerprints for a specific QD structure. This knowledge can be used to address the inverse problem of fitting calculated to measured data by using the QD structure as adjustable parameter.

The paper is organized as follows. First, we describe the interrelation between QD structure, strain, piezoelectricity, and the Coulomb interaction (Sec. II). Then the method of

calculation is outlined, the investigated structures are introduced, and their choice is motivated (Secs. III and IV). The results of the calculations are presented and discussed in Secs. V–VII. The self-consistency corrections and correlation effects are examined more closely in Sec. VIII. Finally, our results are compared to available experimental data in Sec. IX.

II. QD STRUCTURE VERSUS STRAIN, PIEZOELECTRICITY, AND COULOMB INTERACTION

A. Few-particle binding energies

In experiment only energy differences, i.e., recombination energies ω or binding energies Δ_{bind} can be observed. They are related to the ground-state energies of exciton (X^0), biexciton (XX^0), and positive and negative trions ($X^{\pm}$) which are defined by

$$E_0(X^0) = [\mathcal{E}_0^{(e)} - \mathcal{E}_0^{(h)}] + J_{00}^{(eh)} + \delta_{\mathrm{corr}}(X^0) + \delta_{\mathrm{exc}}(X^0),$$

$$E_0(XX^0) = [2\mathcal{E}_0^{(e)} - 2\mathcal{E}_0^{(h)}] + 4J_{00}^{(eh)} + J_{00}^{(ee)} + J_{00}^{(hh)} + \delta_{\mathrm{corr}}(XX^0) + \delta_{\mathrm{exc}}(XX^0),$$

$$E_0(X^-) = [2\mathcal{E}_0^{(e)} - \mathcal{E}_0^{(h)}] + 2J_{00}^{(eh)} + J_{00}^{(ee)} + \delta_{\mathrm{corr}}(X^-) + \delta_{\mathrm{exc}}(X^-),$$

$$E_0(X^+) = [\mathcal{E}_0^{(e)} - 2\mathcal{E}_0^{(h)}] + 2J_{00}^{(eh)} + J_{00}^{(hh)} + \delta_{\mathrm{corr}}(X^+) + \delta_{\mathrm{exc}}(X^+).$$

$E_0(\chi^q)$ is the ground-state energy of particle χ^q including all Coulomb effects. χ is reserved for the number of electron-hole pairs and q for the number and type of spectator charges. The recombination energies $\omega_{00}(\cdot)$ follow from

$$\omega_{00}(X^0 \to 0) = E_0(X^0),$$

$$\omega_{00}(XX^0 \to X^0) = E_0(XX^0) - E_0(X^0),$$

$$\omega_{00}(X^- \to e_0) = E_0(X^-) - \mathcal{E}_0^{(e)},$$

$$\omega_{00}(X^+ \to h_0) = E_0(X^+) + \mathcal{E}_0^{(h)}.$$

The lower indices of $\omega_{00}(\cdot)$ indicate that both the initial and final states are ground states. The binding energies of biexciton, $\Delta_{\mathrm{bind}}(XX^0)$, and trion, $\Delta_{\mathrm{bind}}(X^{\pm})$, are defined with respect to the recombination energy of the exciton ground state as follows:

$$\begin{aligned}\Delta_{\mathrm{bind}}(X^+) &= \omega_{00}(X^0 \to 0) - \omega_{00}(X^+ \to h_0)\\ &= E_0(X^0) - [E_0(X^+) + \mathcal{E}_0^{(h)}]\\ &= -J_{00}^{(eh)} - J_{00}^{(hh)} + \delta_{\mathrm{corr}}(X^0) - \delta_{\mathrm{corr}}(X^+) + \delta_{\mathrm{exc}}(X^0) - \delta_{\mathrm{exc}}(X^+),\end{aligned}$$

$$\begin{aligned}\Delta_{\mathrm{bind}}(X^-) &= \omega_{00}(X^0 \to 0) - \omega_{00}(X^- \to e_0)\\ &= E_0(X^0) - [E_0(X^-) - \mathcal{E}_0^{(e)}]\\ &= -J_{00}^{(eh)} - J_{00}^{(ee)} + \delta_{\mathrm{corr}}(X^0) - \delta_{\mathrm{corr}}(X^-) + \delta_{\mathrm{exc}}(X^0) - \delta_{\mathrm{exc}}(X^-),\end{aligned}$$

$$\begin{aligned}\Delta_{\mathrm{bind}}(XX^0) &= \omega_{00}(X^0 \to 0) - \omega_{00}(XX^0 \to X^0)\\ &= E_0(X^0) - [E_0(XX^0) - E_0(X^0)]\\ &= -2J_{00}^{(eh)} - J_{00}^{(ee)} - J_{00}^{(hh)} + 2\delta_{\mathrm{corr}}(X^0) - \delta_{\mathrm{corr}}(XX^0) + 2\delta_{\mathrm{exc}}(X^0) - \delta_{\mathrm{exc}}(XX^0).\end{aligned} \quad (1)$$

$J_{00}^{(ij)}$ is the direct Coulomb integral between states Ψ_0^i and Ψ_0^j being either electron or hole ground state, $\mathcal{E}_0^{(e/h)}$ is the respective single-particle energies, and $\delta_{\mathrm{corr}}(\chi^q)$ is the energy correction due to self-consistency and correlation effects.

$\delta_{\mathrm{exc}}(\chi^q)$ describes corrections due to exchange. This interaction lifts the fourfold exciton ground-state degeneracy and shifts the biexciton and trion energy. Its energy contribution is very small compared to the direct Coulomb and correlation effects and will be discussed elsewhere. X, XX, and $\omega(\cdot)$ will be used synonymously for X^0, XX^0, and $\omega_{00}(\cdot)$, respectively.

B. Hierarchy of Coulomb effects

Figure 1 depicts the relative importance of the direct Coulomb terms and correlation energies with respect to the binding energies $\Delta(\chi^q)$. Their relation to the QD structure properties will be generally discussed now.

1. Direct Coulomb interaction

The direct Coulomb integrals $J_{00}^{(ij)}$ are calculated employing the Poisson approach,

$$J_{00}^{(ij)} = q_i \int d\mathbf{r} |\Psi_0^i|^2 V_0^j,$$

$$q_j |\Psi_0^j|^2 = \epsilon_0 \nabla \cdot (\epsilon_s \nabla V_0^j). \quad (2)$$

Indices i and j are reserved for the particle type: electron (e) or hole (h). Image charge effects arising from the material-dependent static dielectric constant are taken into account. The magnitude of J depends on the particle types, being either repulsive as for $J_{00}^{(ee)}$ and $J_{00}^{(hh)}$ or attractive such as $J_{00}^{(eh)}$, on the spatial extent of the wave functions and, for $J_{00}^{(eh)}$, on the relative position of electron and hole orbitals. Four different cases with respect to size and position of electron and hole wave functions can arise [Figs. 2(a)–2(d)].

(a) Electron and hole ground-state wave functions share the same barycenter, but the extent of the electron wave function is larger than that of the hole. This is generally considered as the archetype situation for InAs/GaAs QDs, since the resulting order of our four excitonic complexes is thought to be the most typical case encountered in experiment, apart from the antibinding position of the biexciton XX, which results from the so far neglected correlation effect.

(b) A vertical electric field can pull electron and hole apart leading to the configuration displayed in Fig. 2(b).

(c) Reversing the size of electron and hole wave functions leads to the case considered in Fig. 2(c). The resulting order $|J_{00}^{(eh)}| < J_{00}^{(hh)} < J_{00}^{(ee)}$ can also be a consequence of a large piezoelectric field inside the QD, as can be seen from Fig. 8 for large pyramidal QDs. The electron ground-state wave function remains in the QD center, whereas the hole wave func-

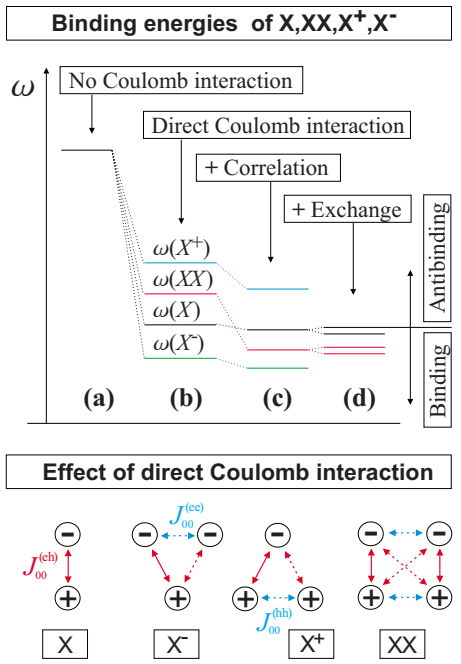

FIG. 1. (Color online) (Upper panel) The evolution of the multiparticle transition energies. (a) No Coulomb interaction is taken into account; the transition energies $\omega(\chi^q)$ are degenerate. (b) Coulomb interaction lifts the degeneracy of the transition energies. Four different combinations in the order of $\omega(\chi^q)$ can occur (see Fig. 2). (c) Adding correlation can result in a binding biexciton. In principle 24 different sequences of $\omega(\chi^q)$ are possible now. (d) Exchange splits the exciton ground state in two nondegenerate dark and two nondegenerate bright states. Since both bright states act as final states for the biexciton decay, $\omega(XX)$ is split as well. (Lower panel) Energetics of the direct Coulomb interaction of the four many-particle states. The appearance of the negative trion X^- decay on the higher- or lower-energy side of the exciton line depends on the relative strength of the additional terms $J_{00}^{(ee)}$ and $J_{00}^{(eh)}$ (additional forces are marked as dashed arrows). If $J_{00}^{(ee)} > |J_{00}^{(eh)}|$ the X^- decay line appears on the high-energy side and otherwise on the low-energy side. The same rationale applies to X^+. For the biexciton XX decay the additional forces are not sufficient to create a binding biexciton since $J_{00}^{(ee)} + J_{00}^{(hh)} \geq 2|J_{00}^{(eh)}|$ always holds.

tion is driven into the two opposite QD edges where the piezoelectric potential has its minimum. The resulting electron-hole overlap decreases and, hence, $|J_{00}^{(eh)}|$ becomes smaller than $J_{00}^{(hh)}$ or $J_{00}^{(ee)}$.

(d) The last possible configuration is electron and hole ground states sharing the same barycenter; but other than in case (a), the electron wave-function extent is smaller than that of the hole state. Typically, QDs with a large vertical aspect ratio feature this type of configuration.

Neglecting correlation, these four cases lead to four different arrangements of the recombination energies $\omega(X)$, $\omega(XX)$, $\omega(X^+)$, and $\omega(X^-)$ as can be seen in Fig. 2 (right panel). $\omega(X)$ is defined as the recombination energy of the first exciton bright state and $\omega(XX)$ as the recombination into the first exciton bright state.

2. Self-consistency, correlation, and exchange

The effect of correlation is more subtle. The hierarchy of Coulomb effects with respect to correlation between electron and hole is schematically shown in Fig. 3. So far the Coulomb integrals are evaluated for fixed single-particle states only [Fig. 3(a)]. By using self-consistent mean-field theory the single-particle orbitals are allowed to alter their shape

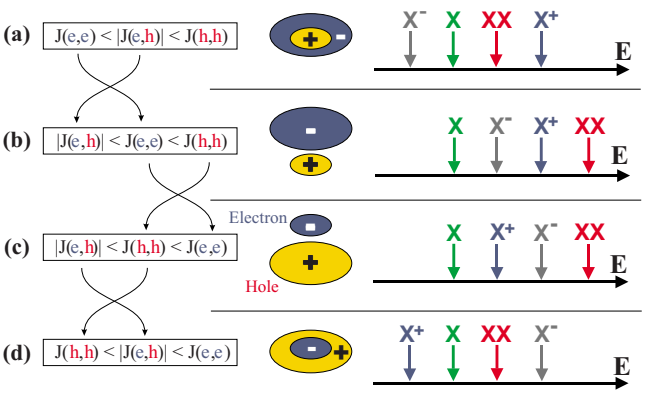

FIG. 2. (Color online) The recombination energy $\omega(\chi^q)$ of X, X^+, and X^- relative to the exciton X (spectroscopic shift) depends in first order on the Coulomb energies $J_{00}^{(eh)}$, $J_{00}^{(ee)}$, and $J_{00}^{(hh)}$. These quantities in turn depend on the electron and hole wave-function sizes and their mutual positions creating four different possibilities labeled with (a)–(d).

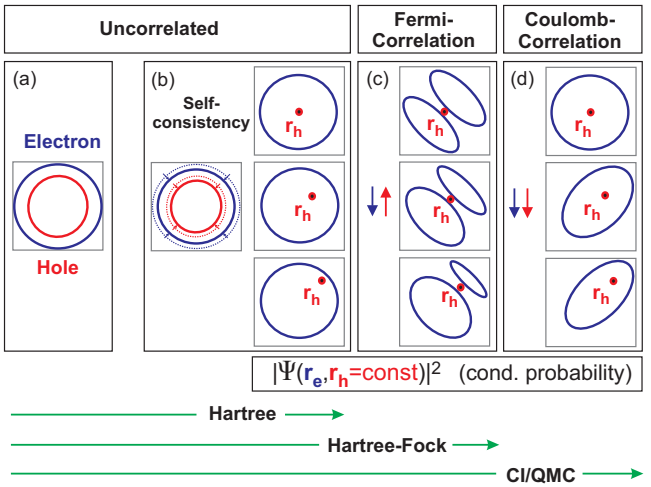

FIG. 3. (Color online) The hierarchy of Coulomb effects and their impact on the electron-hole correlation. (a) Electron and hole as calculated by the single-particle model. The first-order corrections are the direct Coulomb integrals. (b) By employing the Hartree method, electron and hole wave functions shrink to account for the mean-field potential imposed by the respective other carrier. The conditional probability of finding an electron for fixed hole positions, $|\Psi(\mathbf{r}_e, \mathbf{r}_h)|^2$, however, remains unaffected. Hence, electron and hole are still uncorrelated. (c) Both carriers can become correlated by their spin: for opposite spin orientations (for electron-electron interaction: parallel spin orientations) the conditional electron density must vanish at the hole position. Thus, the electron density is anticorrelated with the hole position. This is also known as Fermi correlation and covered by the Hartree-Fock method. (d) For parallel spins, the electron can save Coulomb energy by following the position of the hole. This is called Coulomb correlation and accounted for, e.g., by the CI or the quantum Monte Carlo (QMC) method.

and location in response to Coulomb attraction and repulsion. The Coulomb integrals are solved self-consistently [Fig. 3(b)]. Energy corrections beyond that limit are due to the use of correlated methods such as the configuration-interaction method or the quantum Monte Carlo method. In this case, the probability distribution of one carrier is allowed to become dependent on the positions of the other carriers. This is, e.g., impossible if the excitonic wave function is expressed as a product of electron and hole wave functions only like for the Hartree method. In case of the Hartree-Fock method, the ground state is expressed as a single Slater determinant. Thus, the indistinguishability of fermions is taken into account and exchange effects are included. As a result, electron and hole can become correlated by their spin. This is called Fermi correlation [Fig. 3(c)]. Coulomb correlation is accessible only if linear combinations of multiple Slater determinants are allowed as in the CI method. Then, the probability distribution of finding an electron can follow the position of the hole, in a sense of a conditional probability, as shown in Fig. 3(d). This is also nicely visible in the electron-hole correlation function in the work of Braskén *et al.* (Ref. 9, Fig. 5).

Since we omit the self-consistency step in this paper, the correlation energies in Eq. (1) cover both the correlation energy and the self-consistency corrections. As we will see later in this work, the correlation energy is specific for each particle type and its magnitude can be very different for the various complexes χ^q. Hence, correlation may alter the order of the four transition energies, leading to 24 theoretically possible sequences. An important consequence is the appearance of binding biexcitons, which cannot be achieved by considering direct Coulomb effects alone. As we will see, the magnitude of the corrections is larger, the more dissimilar electron and hole wave functions are and the larger their distance or the smaller their spatial overlap is. Further on, the correlation energies of the four complexes relative to each other depend on the spectral density of electron and hole states.

III. METHOD OF CALCULATION

As soon as more than one charge carrier is confined in the QD, the influence of direct Coulomb interaction, exchange effects, and correlation lead to the formation of distinct multiparticle states. These states are calculated here utilizing the configuration-interaction method. This method rests on a basis expansion of the excitonic Hamiltonians into Slater determinants. These consist of antisymmetrized products of single-particle wave functions obtained from eight-band $\mathbf{k}\cdot\mathbf{p}$ theory in our case. The method is applicable in the strong-confinement regime since the obtained basis functions are already similar to the weakly correlated many-body states.[9,19–21] The eight-band model $\mathbf{k}\cdot\mathbf{p}$ enables us to treat QDs of arbitrary shape and material composition, including the effects of strain, first and second piezoelectricity,[11,13,22] valence-band mixing, and conduction-band–valence-band interaction. The strain enters our model via the use of deformation potentials as outlined by Bahder.[23] Details of the principles of our implementation as well as the parameter set used are outlined in Refs. 11, 12, and 14.

A. Configuration-interaction model

CI is a linear variational method for solving the few-particle Schrödinger equation. Two meanings are connected to the term configuration interaction in this context. Mathematically, configuration simply describes the linear combination of Slater determinants used for the wave functions. In terms of a specification of orbital occupation, interaction means the mixing (interaction) of different electronic configurations (states).

In order to account for correlation, CI uses a wave function $|\Psi_N^\alpha\rangle$ (N is the number of particles and α is an index to label the few-particle states), which is a linear combination of Slater determinants $|\Phi_{a,b,c,\ldots}\rangle$ built up from single-particle orbitals,

$$|\Psi_N^\alpha\rangle = \sum_{a,b,c,\ldots} C_{a,b,c,\ldots}^\alpha |\Phi_{a,b,c,\ldots}\rangle. \tag{3}$$

As an example, the X^+ ground-state configuration (2,2) consists of the two Slater determinants $|\Phi_{e_i,h_1,h_2}\rangle$ with i being the index of the electron ground state ($i \in 1,2$). The wave function results as a linear combination of these two Slater determinants,

$$|\Psi_3^{X+}\rangle = \sum_{i=1}^{2} C_{i,j,k}^{X+} |\Phi_{e_i,h_j,h_k}\rangle \quad (j=1,k=2). \tag{4}$$

If the expansion includes all possible Slater determinants, it is called a full configuration-interaction (FCI) procedure which exactly solves the Schrödinger equation within the space spanned by the one-particle basis set. This is not feasible in our case. Therefore we restrict ourselves to the inclusion of all bound orbitals, where i runs over all confined electron and j,k run over all confined hole states. Still we refer to this approach to as FCI.

Other CI methods use an even more restricted basis set. The allowed Slater determinants can be characterized by the number of excited state orbitals. If only one orbital is excited, it is referred to as a single-excitation determinant (single CI). If one or two excited state orbitals exist it is a single-double excitation determinant [single-double CI (SDCI)] and so on. These derivatives are used to limit the number of determinants in the expansion.

1. Role of the basis size

Since we restrict ourselves to a basis built up from bound orbitals only, part of the correlation energy is not included in our approach. Shumway *et al.*[19] estimated this defect by comparing their FCI results for spherical CdSe QDs having the same restricted expansion basis to a quantum Monte Carlo treatment. They found that their CI calculations cover between 65% and 80% of the total correlation energy, depending on the particle type.

As an example, we compare in Fig. 4 the biexciton correlation energies $\delta_{\mathrm{corr}}(XX)$ for a FCI and a SDCI calculation for an InAs pyramid (17.2 nm base length) as a function of the number of configurations that are taken into account. For the biexciton configurations (2,2), (2,10) (10,2) and the FCI and SDCI are equivalent. Two prominent features are highlighted:

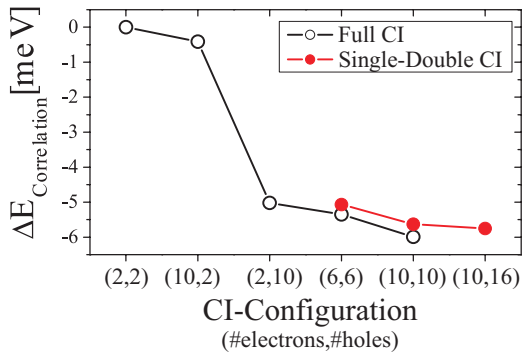

FIG. 4. (Color online) The biexciton correlation energy as a function of the used CI configuration (i,j), where i is the number of electron states and j is the number of hole states being included to build up the CI basis. Results for full CI are compared to that of single-double CI. For the configurations (2,2), (10,2), and (2,10), FCI and SDCI are identical.

First, the correlation energy is much more sensitive to the number of hole states than to the number of electron states, as can be seen by comparing the (2,2)–(2,10) and the (2,2)–(10,2) configurations.

Second, the results for the FCI deviate very little, if at all, from SDCI. The appealing property of the SDCI in this context is the largely reduced number of required matrix elements. For the (10,10) FCI, e.g., eight times more elements are to be evaluated than for the (10,16) SDCI.

The evolution of the basis size with increasing number of carriers is shown in Table I for the full CI method. It highlights the factorial growth in the number of matrix elements, which inhibits the usage of the FCI method for larger number of carriers in an excitonic complex.

In a very recent paper by Troparevsky and Franceschetti[24] an optimized configuration-interaction method was presented that removes the limitations of the conventional approach by identifying the configurations that are most relevant for describing electronic excitations. By using this approach it is conceivable to use not only bound orbitals but also unbound states such as wetting layer, bulk, or hybrid states.

IV. INVESTIGATED STRUCTURES: VARIATION OF SIZE, SHAPE, AND COMPOSITION

Our selection of model QDs is guided by the reported broad variation of structures observed in experiment (see, e.g., Refs. 18 and 25–27 and references therein). The following series are considered (Fig. 5):

TABLE I. Relation between particle type, basis size, number of matrix elements (ME) and number of *nonzero* ME if six electron and ten hole states contribute to the full configuration.

Particle type	Basis size	No. of ME	No. of nonzero ME
X	60	3600	1830
X^-	150	22500	7275
X^+	270	72900	17685
XX	675	455625	63450

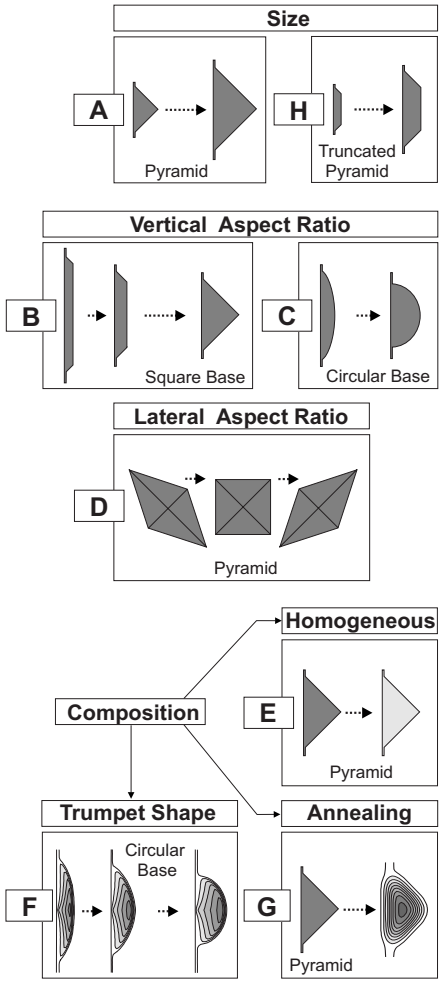

FIG. 5. Structure series investigated in this paper.

Series A: The pyramidal InAs/GaAs structures similar to Ref. 12 with base lengths 10.2 nm (A1), 13.6 nm (A2), 17.0 nm (A3), and 20.4 nm (A4). QDs similar to this series are observed, e.g., by Costantini *et al.*[18] using scanning tunneling microscopy.

Series B: Starting with the 17-nm-base-length pyramid of series A, the vertical aspect ratio ar_V is varied between 0.5 (full pyramid) and 0.04 (very flat QD).

Series C: The QDs have a circular base and their vertical aspect ratio varies between 0.5 (half-sphere) and 0.17.

Series D: Starting again with the 17-nm-base-length pyramid of series A an elongation in [110] and $[1\bar{1}0]$ directions is explored. The lateral aspect ratio ar_L (length in [110] direction divided by length in $[1\bar{1}0]$ direction) varies between 2 and 0.5 (a value of 1 corresponds to the square base). It is important to note that the QD volume has been kept constant for series B, C, and D.

Series E: A homogeneous variation of the In content for $\mathrm{In}_x\mathrm{Ga}_{1-x}\mathrm{As}/\mathrm{GaAs}$ is considered. The starting point again is the 17-nm-base-length pyramid of series A. The In content decreases in steps of 10% from 100% to 70%.

Series F: The QDs of this series have a circular base together with a trumpet-shaped-like InGaAs composition profile (see, e.g., Refs. 16 and 28–30). The integral In amount of the QDs is equal to QD A3.

Series G: By applying a smoothing algorithm on structure A3 with variable smoothing steps (N) the process of Fickian diffusion as a result of an annealing procedure is simulated.

Series H: In addition to the previous list of series we add a special series that is closely related to experiments carried out by Rodt *et al.*[5] and Pohl *et al.*[31] Due to the multimodal distribution of the photoluminescence peaks of the investigated samples, it was possible to derive the structure of the participating QDs to unprecedented detail. It was found that the QDs responsible for each of the nine well-separated peaks differ by one monolayer (ML) in height and base length. The smallest QD starts with a height of three monolayers and a base length of 9.1 nm and the largest one ends with 11 monolayer height and 13.6 nm base length, respectively.

V. IMPACT OF QD SIZE

To study the impact of the QD size we focus on series A and H. The pyramidal shape of the former series represents a model QD structure introduced by Grundmann *et al.*[13] The other series is closely modeled to reproduce the spectroscopic peculiarities observed by Heitz *et al.*[32] describing an onionlike size distribution. Both series together encompass an X^0-energy range of 300 meV starting from 1.3 eV for the smallest QD of series H to as little as 1 eV for the largest full pyramid of series A.

Figure 6 shows the single-particle energies of both series, while Figs. 7 and 8 show the shape of the ground-state wave functions. Their position and spatial extent determine the direct Coulomb energies.

Series H: For the smallest QDs of series H we observe a larger spread of the electron orbital into the surrounding matrix as compared to that of the hole orbital, which is always strongly confined inside the QD. Consequently, the Coulomb repulsion between two electrons is much smaller than for two holes, occupying the ground state. Therefore, the negative trion is binding and the positive trion is antibinding (see Fig. 9). The biexciton is antibinding too since

$$|J_{00}^{(eh)}| < (J_{00}^{(ee)} + J_{00}^{(hh)})/2$$

holds (in case of an equal sign, the biexciton transition would be degenerate with the exciton transition). The smaller the electron-hole size disparity is, the smaller are the binding energies. At a height of 11 ML, the correlation energy $\delta_{\mathrm{corr}}(XX)$ is large enough to create a binding biexciton, although $|\delta_{\mathrm{corr}}(XX)|$ is decreasing with increasing QD height. For the absolute values of the correlation energies we observe the order

$$|\delta_{\mathrm{corr}}(X)| < |\delta_{\mathrm{corr}}(X^-)| < |\delta_{\mathrm{corr}}(XX)| < |\delta_{\mathrm{corr}}(X^+)|.$$

The former two values are increasing and the latter two decreasing upon size increase, however, without changing their order.

Series A: The trend with respect to the relative electron-hole extent continues with series A. For the smallest pyramid of this series the direct Coulomb energies are equal with respect to their absolute value. Hence, the order of the recombination energies is determined by the correlation energies alone. Now we find a binding positive trion and an antibinding negative trion and the biexciton is also in a binding state.

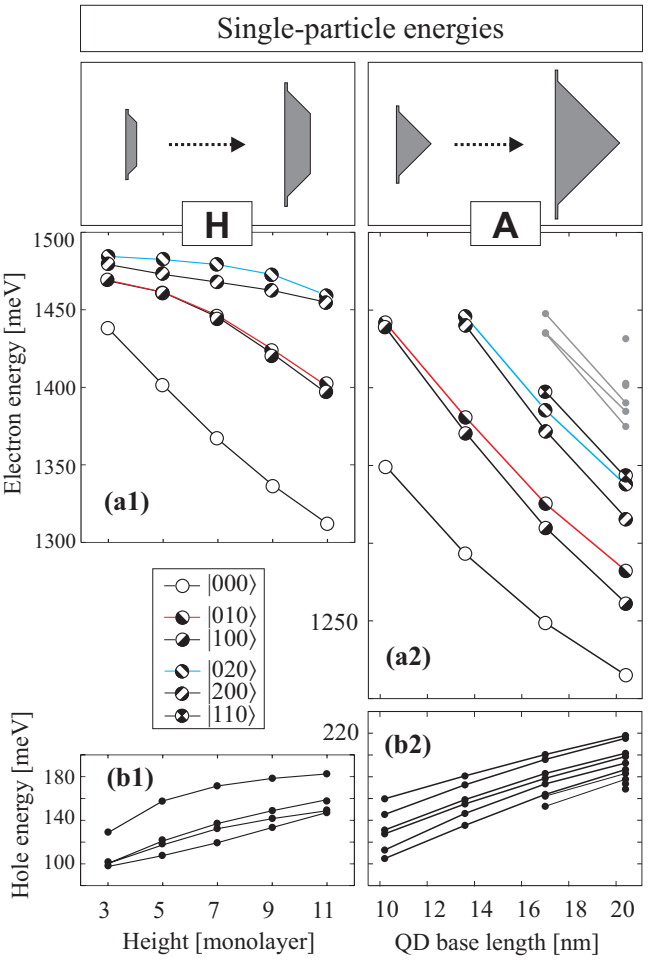

FIG. 6. (Color online) Single-particle electron and hole energies shown for series H and A.

The larger the pyramids of series A become, the larger becomes the hole wave-function extent relative to the electron wave function for two reasons. First, the biaxial strain and its sign change at the QD center enforces a hole position at the QD bottom. Second, since the lateral QD extent is largest at the pyramid base, the hole orbital can cover a comparatively large space larger than the electron orbital can take. This results into a larger Coulomb energy between two electrons than for two holes occupying the ground-state

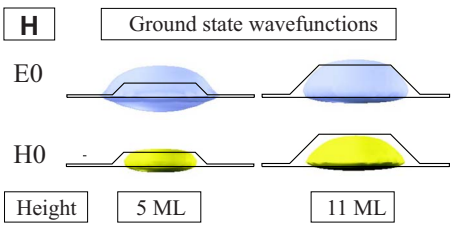

FIG. 7. (Color online) Probability density at 65% of electron and hole ground-state wave functions for QDs of series H having a height of 5 and 11 ML, respectively.

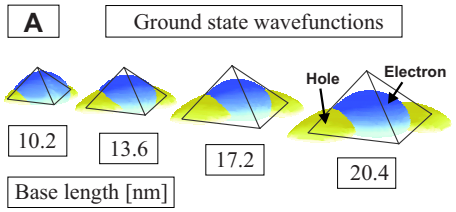

FIG. 8. (Color online) Probability density at 65% of electron and hole ground-state wave functions for pyramidal QDs of series A. Due to the increase in the piezoelectric field with larger QD size the hole wave function tends to elongate along $[1\bar{1}0]$. As a result the electron-hole overlap decreases and $|J_{00}^{(eh)}|$ becomes smaller than $J_{00}^{(hh)}$ and $J_{00}^{(ee)}$.

level. The absolute value of the electron hole Coulomb attraction $|J_{00}^{(eh)}|$ is even smaller than $J_{00}^{(ee)}$ and $J_{00}^{(hh)}$, which results from the piezoelectric field, as will be shown in Sec. V A.

For the correlation energies we observe

$$|\delta_{\mathrm{corr}}(X)| < |\delta_{\mathrm{corr}}(X^-)| < |\delta_{\mathrm{corr}}(XX)| \approx |\delta_{\mathrm{corr}}(X^+)|.$$

The last two quantities exhibit an enormous increase upon increasing pyramid size.

A. Role of the piezoelectric field

In Sec. II A it was demonstrated that the relative size and position of electron and hole wave functions are decisive for the XX, X^+, and X^- binding energies. From our previous work[11,13] we know that the piezoelectric field strongly affects the order and the orientation of the single-particle orbitals and it leads to a spatial separation of electron and hole wave function (see Fig. 8) for series A. As a result, the electron-hole overlap and, hence, their Coulomb attraction decreases and $|J_{00}^{(eh)}|$ can become smaller than $J_{00}^{(ee)}$ and $J_{00}^{(hh)}$ (see, e.g., Table II). Consequently, according to Fig. 2, the XX, X^+, and X^- recombination peaks are blueshifted relative to the exciton line X, as a result of the piezoelectric effect. By taking into account correlation, the picture changes and in most cases we encounter at least a binding positive trion X^+ and sometimes also a binding biexciton XX.

A strong piezoelectric field has a large impact on the shape and orientation of the hole wave functions, especially for the ground state $|h_0\rangle$. In contrast to the electron ground state $|e_0\rangle$, $|h_0\rangle$ is strongly elongated and distorted in the direction of the piezoelectric potential minima. The maximum

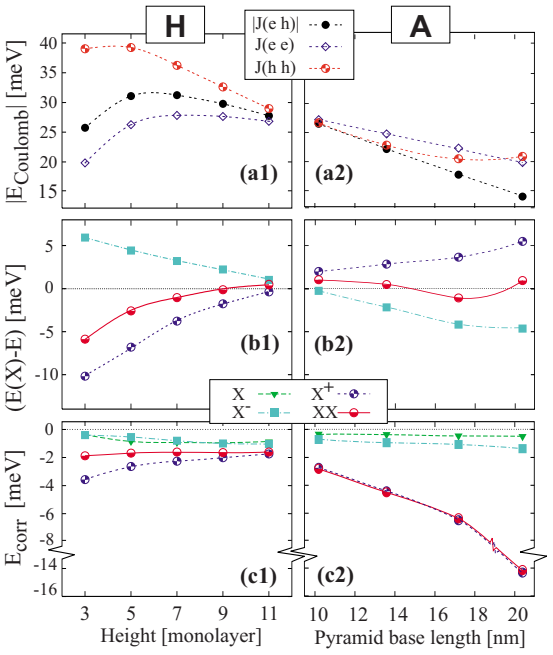

FIG. 9. (Color online) (a) The direct Coulomb energies $J_{00}^{(ee)}$, $J_{00}^{(hh)}$, and $J_{00}^{(eh)}$, (b) the difference of the binding energies with respect to the exciton energy calculated for a configuration $(10e, 10h)$, and (c) the correlation energies $\delta_{\mathrm{corr}}(\chi^q)$ are shown for series A and H. First- and second-order piezoelectric effects are included.

of the probability density of $|h_0\rangle$ resides not in the dot center anymore but is shifted to the corners where the piezoelectric potential has its minimum. Since the probability density increases thereby, the Coulomb repulsion between two holes $J_{00}^{(hh)}$ occupying the ground state is increased. This result is displayed in Table II, where we assess the change in Coulomb and correlation energies for the full pyramid with 17.2 nm base length upon introduction of a piezoelectric field: $|J_{00}^{(eh)}|$ decreases by 1.5 meV and $J_{00}^{(hh)}$ increases by 2.8 meV.

Still the repulsion between two holes remains smaller than for two electrons, $J_{00}^{(hh)} < J_{00}^{(ee)}$, which is a peculiarity of the pyramidal shape, where the special strain conditions force the hole ground state to be located at the QD bottom. Therefore the resulting sequence of Coulomb energies changes from case (d) in Fig. 2 to case (c), along with a crossing of X^+ from binding to antibinding. However, if correlation is added to the calculations, X^+ becomes binding again due to the comparatively large $\delta_{\mathrm{corr}}(X^+)$.

TABLE II. Direct Coulomb, correlation, and binding energies for a (full) pyramidal QD (of base length 17.2 nm) in the (a) absence and (b) presence of the piezoelectric field. For the latter, first- and second-order components are taken into account.

	Coulomb energies (meV)			Correlation energies (meV)		Binding energies (meV)		
	$J_{00}^{(eh)}$	$J_{00}^{(ee)}$	$J_{00}^{(hh)}$	$\delta_{\mathrm{corr}}(XX)$	$\delta_{\mathrm{corr}}(X^+)$	$\Delta_{\mathrm{bind}}(XX)$	$\Delta_{\mathrm{bind}}(X^+)$	$\Delta_{\mathrm{bind}}(X^-)$
(a) Without piezoelectric field	−19.0	22.8	17.7	−3.4	−3.4	−1.3	4.0	−3.9
(b) With piezoelectric field	−17.5	22.5	20.5	−6.4	−6.6	−0.4	3.5	−3.1

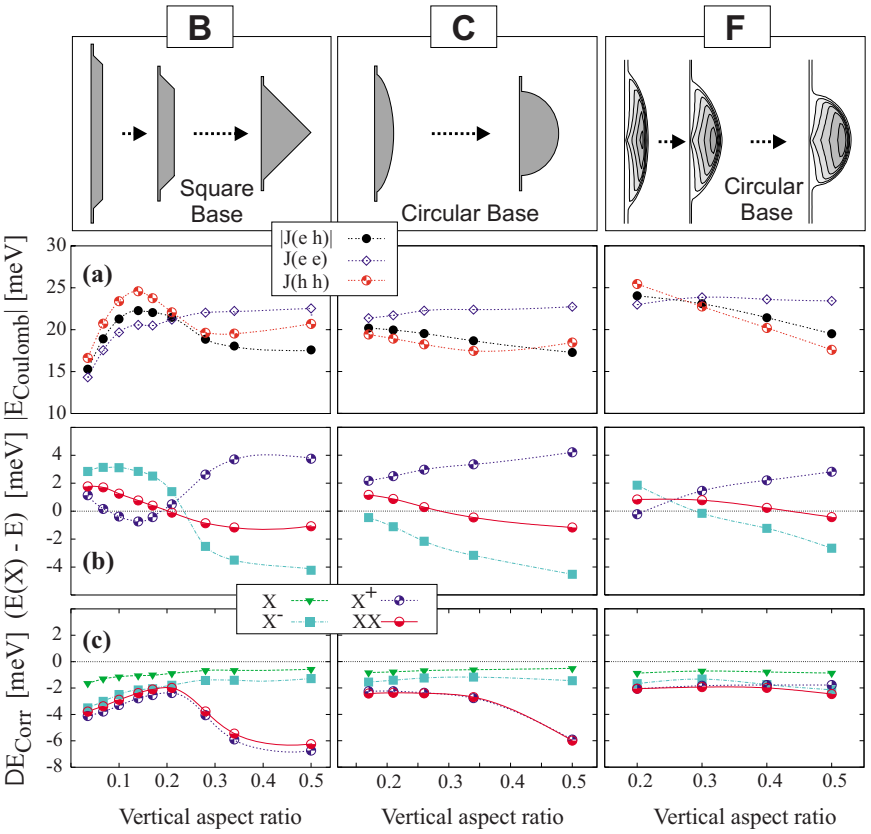

FIG. 10. (Color online) (a) The direct Coulomb energies $J_{00}^{(ee)}$, $J_{00}^{(hh)}$, and $J_{00}^{(eh)}$, (b) the spectroscopic shifts calculated for a configuration $(10e,10h)$, and (c) the degree of correlation shown for series B, C, and F. First- and second-order piezoelectric effects are included.

VI. ASPECT RATIO

A. Vertical aspect ratio

1. Different types of charge separation effects

From Fig. 10 two regimes for series B can be identified in terms of the relative Coulomb binding energies [Fig. 10(a)] and the resulting relative binding energies [Fig. 10(b)]. The first one holds for $\mathrm{ar}_V < 0.2$ and can be described as the unequal vertical wave-function spreadout of electron and hole ground states. Since both share the same barycenter and, apart from their size, have a similar shape, we encounter case (a) of Fig. 2 with the same order of X^+, XX, and X^-. The only difference to Fig. 2(a) is their relative position compared to the exciton, which is changed due to correlation. In this range of ar_V, the very strong z confinement leads to a wave-function spillover of electron and hole states, visible through the decreasing Coulomb energies upon smaller aspect ratio.

The other regime (Stier *et al.*[21] coined the term piezoelectric regime) holds for $\mathrm{ar}_V > 0.2$. It is characterized by a larger hole wave-function extent due to the pyramidal shape (see Sec. V) and a reduced electron hole overlap as a result of a larger piezoelectric field. Hence, the Coulomb attraction of electron and hole $|J_{00}^{(eh)}|$ becomes smaller than $J_{00}^{(ee)}$ or $J_{00}^{(hh)}$.

Series C and F exhibit a similar behavior in terms of the peak order, although the piezoelectricity plays only a minor role in these structures (see Refs. 11 and 22), which becomes visible through the relatively larger electron hole attraction, $|J_{00}^{(eh)}| > J_{00}^{(hh)}$ (except for the half-sphere in series C).

The charge separation in series F is induced by the trumpet-shaped composition profile forcing the hole ground state to be located above the electron ground state. Since the In core extends toward the tip, the hole state can expand in lateral direction more efficiently than the electron. Hence, as in the case of the full pyramid, we find for $\mathrm{ar}_V > 0.2$, $J_{00}^{(ee)} > J_{00}^{(hh)}$.

2. Biexciton binding energy

For all three series B, C, and F, where the vertical aspect ratio is the variation parameter, the biexciton changes from antibinding ($\mathrm{ar}_V = 0.5$) to binding for smaller aspect ratio. The crossover point is different in each series, but the spectroscopic shift is monotonically decreasing with increasing ar_V in all three series.

3. Correlation

Within our three series B, C, and F we again observe that the correlation energies of biexciton and positive trion increase drastically when the attractive Coulomb force $|J_{00}^{(eh)}|$ becomes smaller than the repulsive terms $J_{00}^{(ee)}$ and $J_{00}^{(hh)}$, respectively.

B. Lateral aspect ratio

A QD elongation away from the square basis, as shown in series D, is often discussed as a possible source of the excitonic fine-structure splitting since it introduces a symmetry reduction from C_{4v} to C_{2v} already on the level of the QD structure. However, as long as no piezoelectricity is included (or/and the atomistic symmetry anisotropy (ASA) in the case of atomistic models), there is no distinction possible for the

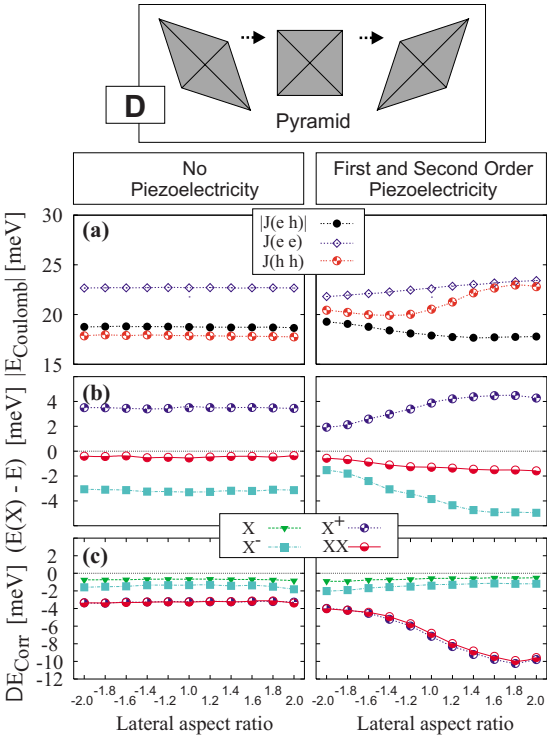

FIG. 11. (Color online) (a) The Coulomb energies $J_{00}^{(ee)}$, $J_{00}^{(hh)}$, and $J_{00}^{(eh)}$, (b) the spectroscopic shifts calculated for a configuration $(10e,10h)$, and (c) the degree of correlation shown for series of elongated QDs (series D) in the cases of excluded piezoelectric field (left panel) and if first- and second-order effects are taken into account (right panel).

single-particle energies or the peak energies of the excitonic spectra between the two possible elongations [110] and $[1\bar{1}0]$. In this case only the polarization delivers the information on the QD orientation. Even more, there is no change in the direct Coulomb energies J and the corresponding few-particle binding energies visible throughout series D, as can be seen in the left panels of Fig. 11.

The situation changes when piezoelectricity is taken into account. (i) First, the electron-hole attraction $J_{00}^{(eh)}$ becomes smaller than the repulsive terms $J_{00}^{(ee)}$ and $J_{00}^{(hh)}$. (ii) Second, the direct Coulomb energies and the resulting binding energies of XX, X^+, and X^- are different for both directions [see Figs. 11(a) and 11(b)]. The order of the excitonic complexes, however, remains unchanged. (iii) The degree of correlation for the biexciton and the positive trion becomes largest for a large elongation along [110], where the attractive electron-hole Coulomb forces reach their minimum and the repulsive Coulomb forces reach their maximum. (iv) Without correlation we observe a completely different order of the excitonic complexes, namely, (X,X^+,X^-,XX) from lower to higher transition energies.

VII. DIFFERENT COMPOSITION PROFILES

A. Inverted conelike composition profile

In order to identify the consequences of an inhomogeneous composition profile like in series F, we compare the flattest QD of this series (ar_V=0.2) (further referred to as $QD_{F\text{-inhom}}^{0.2}$) to the pure InAs lens-shaped QD from series C having the same vertical aspect ratio (further referred to as $QD_{C\text{-hom}}^{0.2}$). Both QDs are designed to contain the same integral amount of InAs. Compared to the archetype pyramidal QD the electron-hole alignment of $QD_{F\text{-inhom}}^{0.2}$ is reversed and their barycenters are 0.2 nm apart. Such a behavior is also found in Stark-shift measurements by Fry *et al.*[30] for structures very similar to model series F.

Prominent differences and similarities between $QD_{C\text{-hom}}^{0.2}$ and $QD_{F\text{-inhom}}^{0.2}$ are as follows:

(i) Both ground-state wave functions (not shown here) of $QD_{F\text{-inhom}}^{0.2}$ are localized stronger than their $QD_{C\text{-hom}}^{0.2}$ counterparts, resulting in significant larger Coulomb energies $J_{00}^{(eh)}$, $J_{00}^{(ee)}$, and $J_{00}^{(hh)}$.

(ii) In contrast to $QD_{C\text{-hom}}^{0.2}$, $J_{00}^{(hh)}$ is larger than $J_{00}^{(ee)}$ for $QD_{F\text{-inhom}}^{0.2}$ since the hole ground state is localized stronger than the electron ground state. Consequently we find a different pattern for the binding energies of XX, X^+, and X^- as can be seen from Fig. 10.

B. Annealed QDs

In series G we simulate the effect of annealing on the electronic properties for a pyramidal QD, originally having a base length of 17.2 nm. Prominent features are the following:

(ii) Both ground-state wave functions increase their localization resulting in larger Coulomb energies $J_{00}^{(eh)}$, $J_{00}^{(ee)}$, and $J_{00}^{(hh)}$.

(ii) Due to the decreasing piezoelectric field upon annealing, $|J_{00}^{(eh)}|$ becomes larger than $J_{00}^{(hh)}$ with the first annealing step. Therefore the biexciton can change its sign and become binding.

(iii) We again observe a dramatic drop of the XX and X^+ correlation energies when $|J_{00}^{(eh)}|$ becomes larger than $J_{00}^{(hh)}$.

C. $In_xGa_{1-x}As$ QDs with uniform composition

A variation of the average $In_xGa_{1-x}As$ composition of QDs is typically employed to tailor the emission wavelength. The impact of the Ga content $(1-x)$ on the multiparticle electronic properties is investigated using series E. From our earlier work[11] we know that with increasing Ga content inside the QD the second-order piezoelectric effect, which dominates for 100% InAs, is reduced. Since the first-order terms remains unaffected we encounter a sign change in the total piezoelectric field.

The presence of piezoelectricity constrains the wave function to a smaller volume leading to an increase in $J_{00}^{(hh)}$. Therefore, we find the smallest value of $J_{00}^{(hh)}$ for a Ga content of 15% (see Fig. 12) where the QD interior is virtually piezoelectric field free. As a result, a nonmonotonic behavior of the biexciton binding energy is observed.

The correlation energies of XX and X^+ exhibit this nonmonotonic behavior too, which is related to the characteristics of $|J_{00}^{(eh)}|-J_{00}^{(hh)}$ turning from negative to positive values first and then to almost zero.

VIII. SELF-CONSISTENCY AND CORRELATION VERSUS QD SIZE, SHAPE, AND PARTICLE TYPE

Self-consistent iteration schemes such as the Hartree method seek to minimize the total energy of few-particle

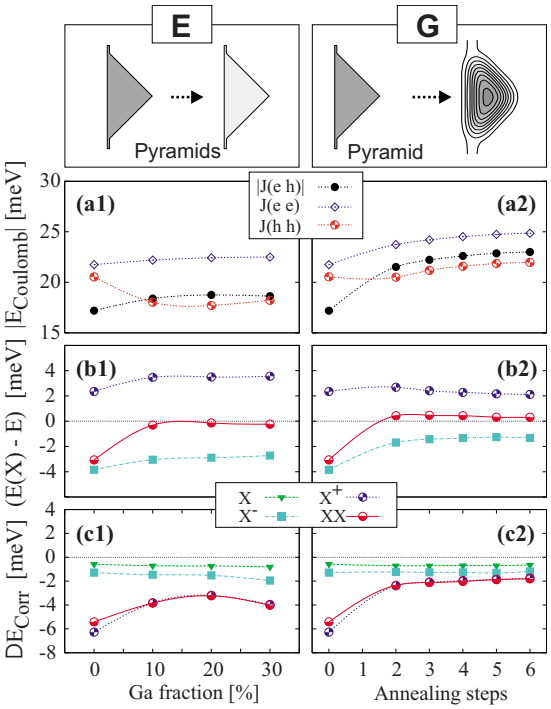

FIG. 12. (Color online) (a) the direct Coulomb energies $J_{00}^{(ee)}$, $J_{00}^{(hh)}$, and $J_{00}^{(eh)}$, (b) the spectroscopic shifts calculated for a configuration $(10e,10h)$, and (c) the degree of correlation shown for series E and G. First- and second-order piezoelectric effects are included.

complexes in a tradeoff between the kinetic and potential energies of the involved single-particle states and their mutual Coulomb attraction or repulsion in the mean-field approximation. Beyond the mean-field approximation, exchange and correlation effects come into play. Then, the probability distribution of finding one carrier at a certain position becomes dependent on the *positions* of the other carriers in the sense of conditional probabilities.

From Figs. 9–11 and 12(c) it can be seen that the magnitude of these correction is specific for each particle type and foremost dependent on the QD size and shape. This is particularly obvious in series A (see Fig. 9), where $|\delta_{\mathrm{corr}}(XX)| \approx |\delta_{\mathrm{corr}}(X^+)| > |\delta_{\mathrm{corr}}(X^-)| > |\delta_{\mathrm{corr}}(X)|$ and all the correlation energies increase with increasing dot size.

In general, there are three main factors, which determine the magnitude of self-consistency corrections and degree of correlation:

(i) First, the absolute and relative size of electron and hole wave functions and their mutual position; in other words, how much Coulomb energy can be gained $(J^{(eh)})$ or saved $(J^{(hh)}, J^{(ee)})$ by relocating to a more favorable place, changing shape or size. We observe, for instance, strong correlation effects for the positive trion and biexciton in the following cases:

(1) Electron and hole orbital sizes are very dissimilar like in series H due to the asymmetric spreadout of electron and hole wave functions. (2) The barycenters of both carriers are at different vertical positions as in the case of the half-sphere. We find a dipole of 1.5 nm resulting in a smaller Coulomb attraction between electron and hole $J_{00}^{(eh)}$ compared to $J_{00}^{(ee)}$ and $J_{00}^{(hh)}$ [Fig. 10(c)]. (3) The largest correlation energies are observed for the largest full pyramid of series A. Electron and hole orbitals are pulled into different directions due to strong piezoelectricity. Their spatial overlap reduces and $J_{00}^{(eh)}$ becomes smaller than $J_{00}^{(ee)}$ and $J_{00}^{(hh)}$. For this case we observe correlation energies on the order of 15 meV. This large value, however, is also related to the large wave-function extent and the accompanying small kinetic energy. This will be further detailed below in case (iii).

(ii) Second, the particle type. Here, the ratio of the number of Coulomb interactions within a particle type to the number of carriers within this complex is of importance. Since the CI method is a variational method, this ratio weights the importance of the Coulomb interaction relative to the kinetic energies of the single carriers. For the exciton this ratio is 1/2, one Coulomb integral compared to two carriers. For the biexciton we have the ratio of 6/4, six Coulomb integrals and four particles. Therefore, the relative importance of the Coulomb interaction is larger for the biexciton than for the exciton and, hence, more emphasis is put on minimizing the total Coulomb energy in the case of the biexciton, which is done by mixing higher excited state configurations into the CI ground state.

For both trions we encounter a ratio of 3/3, three Coulomb integrals and three particles. Hence, this point cannot explain why the correlation energies are mostly very different for the positive and the negative trions, which will be explained by the next point.

(iii) Third, the sensitivity of the kinetic energy to small wave-function size variations or equivalently the unequal density of the electron and hole spectra. Both quantities are functions of the effective mass and the spatial wave-function extent. A larger effective mass translates into a smaller kinetic energy and a smaller energetic separation of ground and excited states. A larger wave-function extent in real space transforms in a smaller extent in k space; hence, the kinetic-energy integral

$$E_{\mathrm{kin}} \approx \int_{V_k} \Psi^*(\mathbf{k}) E(\mathbf{k}) \Psi(\mathbf{k}) d\mathbf{k},$$

becomes smaller too. Consequently, variations δE_{kin}, resulting from small size variations of the wave functions, are larger for steep dispersions $E(\mathbf{k})$, i.e. small effective masses, and small wave functions extents. In other words, δE_{kin} is large for small electrons and small for large hole orbitals. If δE_{kin} is small, the wave function can more easily reshape to save Coulomb energy. The "reshaping" in our case is performed by mixing higher excited state configurations into the ground-state configuration.

The importance of this point becomes visible by comparing $\delta_{\mathrm{corr}}(X^+)$ and $\delta_{\mathrm{corr}}(X^-)$. Both complexes $X^+(h_0^2 e_0^1)$ and $X^-(h_0^1 e_0^2)$ share the same number of particles but in different configurations. Since the density of the hole spectrum is larger than that of the electron spectrum, the energy of those complexes, containing a larger number of positive carriers, is more affected by correlation. Therefore, $\delta_{\mathrm{corr}}(X^+) > \delta_{\mathrm{corr}}(X^-)$ holds. The denser the spectrum becomes, the larger can be the correlation, as can be seen from the rising correlation

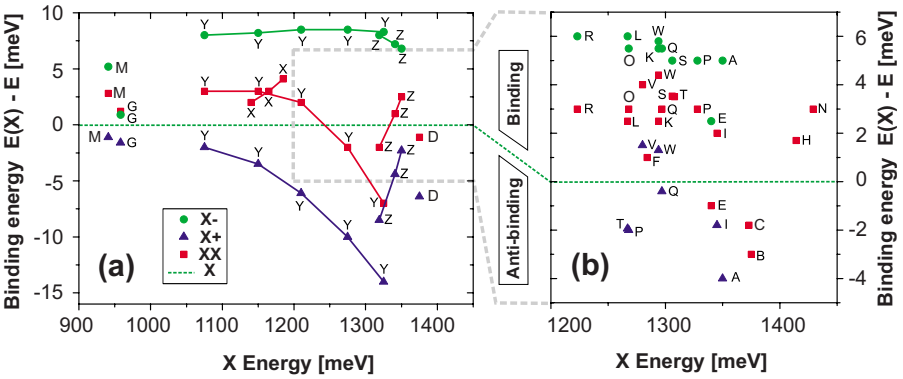

FIG. 13. (Color online) Compilation of measured binding energies, $\Delta_{\mathrm{bind}}(\cdot)$ (see Table III) found in literature. The capital letters link the data point to the reference given in Table III (first column). Letters X, Y, and Z refer to series of data points, where only representative values are shown in this graph.

energies of series A with increasing size in Fig. 9 (the corresponding spectral density can be derived from Fig. 6).

Another striking example is series B. Here, the absolute *and* the relative spectral densities change with the aspect ratio. For the pyramid (ar_V=0.5) again we observe a large spectral hole density and small electron density. The electron density (see Ref. 11) becomes larger with smaller aspect ratio resulting in a rising correlation energy of X and X^-. The hole density in contrast becomes smaller until ar_V=0.1. Below that value the spectral hole density is rising again. This translates into a nonmonotonic δ_{corr} behavior of the particles containing two holes: XX and X^+ [see Fig. 10(c)1].

IX. COMPARISON TO EXPERIMENT

In this section we compare our theoretical findings with available single-dot spectroscopic data, which are compiled in Fig. 13 and Table III. Our goal is complicated by the following obstacles. (i) QDs for practical application preferably emit at around 1 eV, whereas the available single-dot spectra are mostly recorded above 1.2 eV. The spectral range above this value is better accessible due to the availability of very sensitive low-noise Si detectors. InGaAs detectors for the energy range below 1.2 eV down to 0.8 eV, in contrast, require much larger integration times due to the large noise. Since most of our model structures are predicted to emit below 1.2 eV (see Fig. 14 and Ref. 11) experimental data are not always available for comparison. (ii) Only in rare cases we find spectroscopic investigations accompanied by high-resolution structural data or comparable information.

The experimental data in Table III, exciton energies, and binding energies of XX,X^+,X^- are sorted according to the biexciton binding energies, which vary between −8 and 5 meV. The binding energies of the negative trion, $\Delta_{\mathrm{bind}}(X^-)$, are always positive (binding); those of the positive trion, $\Delta_{\mathrm{bind}}(X^+)$, are negative (antibinding) except in case V (Ref. 49) and W.[50] The latter "exceptions" come along with the largest biexciton binding energies. In the last column we provide an ordering index as introduced in Table IV. Out of 24 possible arrangements for the particles X,XX,X^+,X^- only four are identified so far in experiment: 0, 1, 6, and 7. The last three are nondirect-Coulomb-only configurations; in other words, they can be interpreted only by taking into account correlation effects. The configurations with indices 0, 1, and 6 also appear in our calculations. Configuration 7 stems from a QD, embedded in a quantum well, which is not considered in this work.

Effect of QD size. The experimental data labeled Y differ from the other ones in several aspects. First, the exciton energies cover a range of approximately 250 meV. Second, the magnitude of the splittings between the four peaks is much larger, and, third, detailed structural information is available. The latter forms the basis for the design of our model series H. Besides the peculiar QD size distribution, in particular the high InAs content yields the strong energy splittings. The result of our model calculations for series H agree very well, qualitatively and, to a large degree, even quantitatively with the measured values [see Fig. 9(b)1].

Effect of annealing. The experimental data labeled by letter Z are obtained during the annealing of 1 and the same QD. The energy splitting between biexciton and trions strongly decreases and a biexciton binding-antibinding crossover occurs. This transition is nicely reproduced by our annealing series G [see Fig. 12(b)2] which we attribute to the reduction in the net piezoelectric field during the annealing process. For the unannealed starting QD in our model series G, which has sharp interfaces, the second-order piezoelectric field surpasses the first-order field. This results in a sizeable net piezoelectric potential, which separates electron and hole wave functions leading to an antibinding biexciton. The subsequent annealing process softens the interfaces, reduces the strain near the interfaces, and hence decreases the second-order piezoelectric field. As a result, first- and second-order components compensate, the electron-hole separation becomes smaller, and the biexciton becomes binding.

For this particular experiment, however, series G is not a good model structure since it predicts the wrong trion order. This, however, can be fixed by taking a QD from series H as starting point for the annealing series, as we did in Ref. 53.

The spectroscopic annealing data provide the link between the pure InAs QDs of series Y and the majority of the experimental data found in literature [see Fig. 13(b)]. It appears that the favored growth modes produce highly intermixed QDs. Transmission electron microscopy data of such QDs (Refs. 28 and 29) confirm this assumption. Moreover, they often exhibit a trumpet-shaped-like In distribution inside the QD and a small vertical aspect ratio, thus resembling the flat structure of our model series F. For this model QD we find the same peak order as for the majority of the experimental data plotted in Fig. 13(b), [K-M,O-T].

TABLE III. Compilation of experimental results for the binding energies of biexciton, $\Delta_{\text{bind}}(XX)$, positive trion, $\Delta_{\text{bind}}(X^+)$, and negative trion, $\Delta_{\text{bind}}(X^-)$. The host material is always GaAs. The Id in the first column is used to identify the reference in Fig. 13. In the last column an ordering index as introduced in Table IV is provided. Index numbers in parentheses are estimated assuming either positive (+) $\Delta_{\text{bind}}(X^-)$ or negative (–) $\Delta_{\text{bind}}(X^+)$ trion binding energies, if one of them is missing in experiment.

Id	Reference	$E_0(X_0)$ (meV)	$E(X_0-X_p)$ (meV)	$\Delta_{\text{bind}}(XX)$ (meV)	$\Delta_{\text{bind}}(X^-)$ (meV)	$\Delta_{\text{bind}}(X^+)$ (meV)	Estimated size, QD material	Index
A	33	1350	40		5	–4	40×3, InGaAs	
B	34	1375		–3			InGaAs	
C	35	1373		–1.8			InGaAs	
D	36	1375		–1.1	(+)	–6.4	InGaAs	(0)
E	37	1340		–1	2.5[a]		[10,12]×4, InGaAs	
F	38	1284	40	1			45×4.5, InGaAs	
G	39	958		1.2	0.9	–1.6	In(Ga)As in In(15)Ga(85)As quantum well	7
H	40	1414		1.7			$In_xGa_{1-x}As/GaAs$, high-temp. cap	
I	41	1345	40	2		–1.8	InGaAs	
K	7	1294		2.5	5.5	(–)	InGaAs	(1)
L	42	1267	60	2.5	6	–2	InGaAs	1
M	43	941		2.8	5.2	–1.1	InAs in 5 nm InGaAs quantum well	1
N	2	1429		3			InGaAs	
O	6	1268	45[a]	3[a]	5.5	–2	InGaAs	1
P	44	1328		3	5	(–)	InGaAs	(1)
Q	45	1297		3	5.5	–0.4	InGaAs	1
R	46	1223	35	3[a]	6[a]	(–)	InGaAs	(1)
S	47	1306		3.5[a]	5	(–)	InGaAs	(1)
T	48	1308		3.5			45×3, InGaAs	
V	49	1280		4		1.5	24×3, InGaAs	
W	50	1294		4.4	5.8	1.3	24×3, InGaAs	6
X	51	[1130, 1200]		[2–4.5]			InAs in InGaAs quantum well	
Y	5 and 52	[1075, 1350]	[75–120]	[–8–5]	[7.5–9]	[–14–-0.5]	Almost pure InAs in GaAs	0;1
Z	53	[1319, 1350]		[–2–2.5]	[6.8–8]	[–8.5–-2.3]	InGaAs	0;1

[a]Estimated value.

X. INVERSION PROBLEM

In Fig. 14 we compiled some of our data to visualize the wealth in the variation of the spectroscopic properties for different QD structures. The difference between the exciton *s*- and *p*-channel transitions as a function of the exciton energy (an easy observable quantity in experiment) is a meaningful parameter to distinguish between different types of $In_xGa_{1-x}As/GaAs$ QD structures. The attached symbols, in addition, carry the information about the ordering of the $X, XX, X^{\pm}$ resonances.

The idea behind the inversion problem is the following. If two QDs had the same electronic energy spectrum they need to be described by the same Hamiltonian. That means they were morphologically identical. In experiment, however, only a subset of the spectrum, additionally masked by Coulomb interaction, is observable. For example, a given exciton energy can be produced by a large manifold of QD structures spanned by simultaneous variations of size, shape, and composition. Within this manifold, however, the binding energies of the other excitonic complexes, such as the biexciton or the trion, are different. Hence, their knowledge contributes complementary information. The subset of QDs having not only the same exciton energy but also the same splitting of the *s*-*p*-channel transitions and the same binding energies for biexciton and the trions is much smaller, but we cannot prove that for this specific choice of parameters the subset reduces to one definite QD structure.

In Fig. 14, for example, we find seven very different QD structures in the exciton energy range between 1150 and 1175 meV. If one additionally introduces a restriction on the *s*-*p*-channel spacing to values between 105 and 115 meV, still two QDs remain: one is a truncated InAs pyramid with abrupt interfaces from series H and a strongly annealed QD with very smooth interfaces from series G. The different symbols attached to the data points, however, indicate a very different ordering of the few-particle resonances. Hence, only the different spectroscopic shifts lead to the distinction between the remaining two structures.

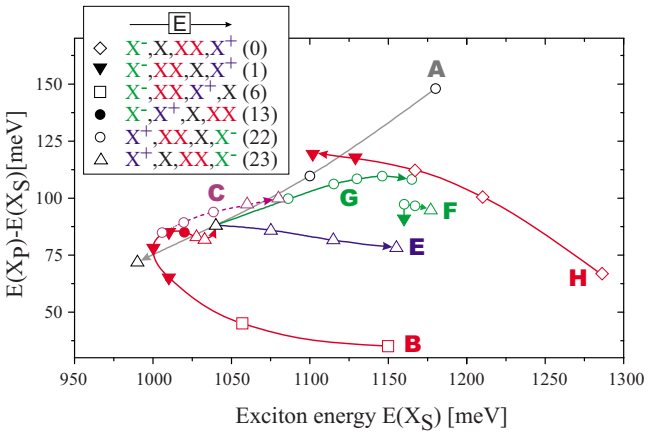

FIG. 14. (Color online) The difference $[E(X_p)-E(X_s)]$ plotted versus $E(X_s)$. With $E(X_p)$ we denote the average value of the p-channel transitions taken from the excitonic absorption spectra. The data are shown for the series A–C and E–H. The symbols are used to denote the order of the calculated few-particle resonances, X, XX, and $X^{\pm}$. The small arrows indicate the order of structures within each series as shown in the structure figures attached to the electronic data (Figs. 6, 10, and 12). The numbers in parentheses are related to the ordering index introduced in Table IV.

XI. CONCLUSIONS

For a large number of QD structures of varying size, shape, and composition we investigated the relationship between the structural properties and the energies of a selected set of few-particle states $(X,XX,X^{\pm})$, which can be easily traced in experiment. The resulting binding energies turn out to be very sensitive to the various morphological peculiarities. We analyzed in detail the relationship between the QD geometry, the resulting shape and position of electron and hole wave functions, the direct Coulomb energies, and changes introduced by self-consistency and correlation effects. The correlation effects are larger for biexciton and positive trion states, which we attribute to the larger spectral density of the hole subsystem. This in turn is a result of the larger hole effective mass. Correlation is very sensitive to the relative size and position of the electron and hole ground-state orbitals, influencing equally the direct Coulomb energies $J_{00}^{(eh)}$, $J_{00}^{(ee)}$, and $J_{00}^{(hh)}$. Large correlation energies $\delta_{\mathrm{corr}}(XX)$ and $\delta_{\mathrm{corr}}(X^{+})$ are observed in those cases, where the absolute value of the attractive Coulomb term $J_{00}^{(eh)}$ falls below the values of the repulsive terms $J_{00}^{(ee)}$ and $J_{00}^{(hh)}$.

We have addressed the band-structure inversion problem for quantum dots. In Fig. 14 we compiled some of our data to visualize the wealth in the variation of the spectroscopic properties for different QD structures. We found the difference between the exciton s- and p-channel transitions as a function of the exciton energy (an easy observable quantity in experiment) a meaningful fingerprint in order to distinguish between different types of $In_xGa_{1-x}As/GaAs$ QD structures. If, in addition, complementary data on the spectroscopic shifts of $XX,X^{\pm}$ relative to X are available, we are quite confident that, by the spectroscopic signature alone, the space of possible QD morphologies can be strongly reduced.

TABLE IV. The sequence of the $X,XX,X^{\pm}$ peaks can be arranged in 24 different combinations. Four of them (a)–(d) can form by taking the direct Coulomb interaction into account only. For the other 20 combinations it additionally requires correlation to establish. With proximity $\alpha i, \alpha \in \{a,b,c,d\}$, we intend to describe how many transpositions i it requires to end up in of the pure Coulomb cases (a), (b), (c), or (d). The 24 cases are labeled with a unique index. The bold indices refer to the combinations we find in this work for our investigated structures.

Order of appearance				proximity to case	Index
1	2	3	4	**(a), (b), (c), (d)**	
X^-	X	XX	X^+	(a)	**0**
X^-	XX	X	X^+	(a1)	**1**
X^-	X^+	XX	X	(a1)	2
XX	X	X^-	X^+	(a1)	3
X^-	X	X^+	XX	(a1), (b1)	4
X	X^-	XX	X^+	(a1), (b1)	5
X^-	XX	X^+	X	(a2), (b2)	**6**
XX	X^-	X	X^+	(a2), (b2)	7
X	XX	X^+	X^-	(b1)	8
XX	X^-	X^+	X	(b1)	9
X^+	X^-	X	XX	(b1)	10
X	X^-	X^+	XX	(b)	11
X	X^+	X^-	XX	(c)	12
X^-	X^+	X	XX	(c1)	**13**
X	XX	X^-	X^+	(c1)	14
XX	X^+	X^-	X	(c1)	15
X	X^+	XX	X^-	(c1), (d1)	16
X^+	X	X^-	XX	(c1), (d1)	17
XX	X^+	X	X^-	(c2), (d2)	18
X^+	XX	X^-	X	(c2), (d2)	19
XX	X	X^+	X^-	(d1)	20
X^+	X^-	XX	X	(d1)	21
X^+	XX	X	X^-	(d1)	**22**
X^+	X	XX	X^-	(d)	**23**

ACKNOWLEDGMENTS

We acknowledge many fruitful discussions with R. Zimmermann, S. Rodt, R. Seguin, and G. Bester. This work was funded by SFB 787 of DFG. The calculations were performed on a IBM p690 supercomputer at the HLRN Berlin/Hannover.

*andrei@sol.physik.tu-berlin.de

[1] R. Seguin, A. Schliwa, S. Rodt, K. Pötschke, U. W. Pohl, and D. Bimberg, Phys. Rev. Lett. **95**, 257402 (2005).

[2] M. Bayer, T. Gutbrod, A. Forchel, V. D. Kulakovskii, A. Gorbunov, M. Michel, R. Steffen, and K. H. Wang, Phys. Rev. B **58**, 4740 (1998).

[3] S. Rodt, R. Heitz, A. Schliwa, R. L. Sellin, F. Guffarth, and D. Bimberg, Phys. Rev. B **68**, 035331 (2003).

[4] L. Landin, M. S. Miller, M. Pistol, C. E. Pryor, and L. Samuelson, Science **280**, 262 (1998).

[5] S. Rodt, A. Schliwa, K. Pötschke, F. Guffarth, and D. Bimberg, Phys. Rev. B **71**, 155325 (2005).

[6] M. E. Ware, A. S. Bracker, E. Stinaff, D. Gammon, D. Gershoni, and V. L. Korenev, Physica E **26**, 55 (2005).

[7] B. Urbaszek, R. J. Warburton, K. Karrai, B. D. Gerardot, P. M. Petroff, and J. M. Garcia, Phys. Rev. Lett. **90**, 247403 (2003).

[8] G. A. Narvaez, G. Bester, and A. Zunger, Phys. Rev. B **72**, 245318 (2005).

[9] M. Braskén, M. Lindberg, D. Sundholm, and J. Olsen, Phys. Rev. B **61**, 7652 (2000).

[10] G. Bester, X. Wu, D. Vanderbilt, and A. Zunger, Phys. Rev. Lett. **96**, 187602 (2006).

[11] A. Schliwa, M. Winkelnkemper, and D. Bimberg, Phys. Rev. B **76**, 205324 (2007).

[12] O. Stier, M. Grundmann, and D. Bimberg, Phys. Rev. B **59**, 5688 (1999).

[13] M. Grundmann, O. Stier, and D. Bimberg, Phys. Rev. B **52**, 11969 (1995).

[14] O. Stier and D. Bimberg, Phys. Rev. B **55**, 7726 (1997).

[15] H. Eisele, O. Flebbe, T. Kalka, C. Preinesberger, F. Heinrichsdorff, A. Krost, D. Bimberg, and M. Dähne Prietsch, Appl. Phys. Lett. **75**, 106 (1999).

[16] D. M. Bruls, J. W. A. M. Vugs, P. M. Koenraad, H. W. M. Salemink, J. H. Wolter, M. Hopkinson, M. S. Skolnick, F. Long, and S. P. A. Gill, Appl. Phys. Lett. **81**, 1708 (2002).

[17] J. Marquez, L. Geelhaar, and K. Jacobi, Appl. Phys. Lett. **78**, 2309 (2001).

[18] G. Costantini, A. Rastelli, C. Manzano, R. Songmuang, O. G. Schmidt, K. Kern, and H. von Känel, Appl. Phys. Lett. **85**, 5673 (2004).

[19] J. Shumway, A. Franceschetti, and A. Zunger, Phys. Rev. B **63**, 155316 (2001).

[20] G. Bester, S. Nair, and A. Zunger, Phys. Rev. B **67**, 161306(R) (2003).

[21] O. Stier, A. Schliwa, R. Heitz, M. Grundmann, and D. Bimberg, Phys. Status Solidi B **224**, 115 (2001).

[22] G. Bester, A. Zunger, X. Wu, and D. Vanderbilt, Phys. Rev. B **74**, 081305(R) (2006).

[23] T. B. Bahder, Phys. Rev. B **41**, 11992 (1990).

[24] M. Troparevsky, and A. Franceschetti, J. Phys.: Condens. Matter **20**, 055211 (2008).

[25] S. Ruvimov *et al.*, Phys. Rev. B **51**, 14766 (1995).

[26] A. Lenz, R. Timm, H. Eisele, Ch. Hennig, S. K. Becker, R. L. Sellin, U. W. Pohl, D. Bimberg, and M. Dähne, Appl. Phys. Lett. **81**, 5150 (2002).

[27] Q. Gong, P. Offermans, R. Nötzel, P. M. Koenraad, and J. H. Wolter, Appl. Phys. Lett. **85**, 5697 (2004).

[28] N. Liu, J. Tersoff, O. Baklenov, A. L. Holmes, and C. K. Shih, Phys. Rev. Lett. **84**, 334 (2000).

[29] T. Walther, A. G. Cullis, D. J. Norris, and M. Hopkinson, Phys. Rev. Lett. **86**, 2381 (2001).

[30] P. W. Fry *et al.*, Phys. Rev. Lett. **84**, 733 (2000).

[31] U. W. Pohl, K. Pötschke, A. Schliwa, F. Guffarth, D. Bimberg, N. D. Zakharov, P. Werner, M. B. Lifshits, V. A. Shchukin, and D. E. Jesson, Phys. Rev. B **72**, 245332 (2005).

[32] R. Heitz, F. Guffarth, K. Pötschke, A. Schliwa, D. Bimberg, N. D. Zakharov, and P. Werner, Phys. Rev. B **71**, 045325 (2005).

[33] D. V. Regelman, E. Dekel, D. Gershoni, E. Ehrenfreund, A. J. Williamson, J. Shumway, A. Zunger, W. V. Schoenfeld, and P. M. Petroff, Phys. Rev. B **64**, 165301 (2001).

[34] E. Moreau, I. Robert, L. Manin, V. Thierry-Mieg, J. M. Gérard, and I. Abram, Phys. Rev. Lett. **87**, 183601 (2001).

[35] M. Persson, N. Panev, L. Landin, S. Jeppesen, and M.-E. Pistol, Phys. Rev. B **64**, 075309 (2001).

[36] R. M. Thompson, R. M. Stevenson, A. J. Shields, I. Farrer, C. J. Lobo, D. A. Ritchie, M. L. Leadbeater, and M. Pepper, Phys. Rev. B **64**, 201302(R) (2001).

[37] L. Landin, M.-E. Pistol, C. Pryor, M. Persson, L. Samuelson, and M. Miller, Phys. Rev. B **60**, 16640 (1999).

[38] E. Dekel, D. V. Regelman, D. Gershoni, E. Ehrenfreund, W. V. Schoenfeld, and P. M. Petroff, Phys. Rev. B **62**, 11038 (2000).

[39] B. Alloing, C. Zinoni, V. Zwiller, L. H. Li, C. Monat, M. Gobet, G. Buchs, A. Fiore, E. Pelucchi, and E. Kapon, Appl. Phys. Lett. **86**, 101908 (2005).

[40] C. Santori, M. Pelton, G. Solomon, Y. Dale, and Y. Yamamoto, Phys. Rev. Lett. **86**, 1502 (2001).

[41] J. J. Finley, A. D. Ashmore, A. Lemaître, D. J. Mowbray, M. S. Skolnick, I. E. Itskevich, P. A. Maksym, M. Hopkinson, and T. F. Krauss, Phys. Rev. B **63**, 073307 (2001).

[42] M. E. Ware, E. A. Stinaff, D. Gammon, M. F. Doty, A. S. Bracker, D. Gershoni, V. L. Korenev, Ş. C. Bădescu, Y. Lyanda-Geller, and T. L. Reinecke, Phys. Rev. Lett. **95**, 177403 (2005).

[43] N. I. Cade, H. Gotoh, H. Kamada, H. Nakano, and H. Okamoto, Phys. Rev. B **73**, 115322 (2006).

[44] W.-H. Chang, H.-S. Chang, W.-Y. Chen, T. M. Hsu, T.-P. Hsieh, J.-I. Chyi, and N.-T. Yeh, Phys. Rev. B **72**, 233302 (2005).

[45] M. Ediger, P. Dalgarno, J. Smith, B. Gerardot, R. Warburton, K. Karrai, and P. Petroff, Appl. Phys. Lett. **86**, 211909 (2005).

[46] M. Lomascolo *et al.*, Phys. Rev. B **66**, 041302(R) (2002).

[47] F. Findeis, M. Baier, E. Beham, A. Zrenner, and G. Abstreiter, Appl. Phys. Lett. **78**, 2958 (2001).

[48] A. Kiraz, S. Fálth, C. Becher, B. Gayral, W. V. Schoenfeld, P. M. Petroff, L. Zhang, E. Hu, and A. Imamoğlu, Phys. Rev. B **65**, 161303(R) (2002).

[49] N. Akopian, N. H. Lindner, E. Poem, Y. Berlatzky, J. Avron, D. Gershoni, B. D. Gerardot, and P. M. Petroff, Phys. Rev. Lett. **96**, 130501 (2006).

[50] E. Poem, J. Shemesh, I. Marderfeld, D. Galushko, N. Akopian, D. Gershoni, B. D. Gerardot, A. Badolato, and P. M. Petroff, Phys. Rev. B **76**, 235304 (2007).

[51] C. Dal Savio, K. Pierz, G. Ade, H. Danzebrink, E. Göbel, and A. Hangleiter, Appl. Phys. B: Lasers Opt. **84**, 317 (2006).

[52] S. Rodt, R. Seguin, A. Schliwa, F. Guffarth, K. Pötschke, U. Pohl, and D. Bimberg, J. Lumin. **122-123**, 735 (2007).

[53] R. Seguin *et al.*, Appl. Phys. Lett. **89**, 263109 (2006).